

CRUSTAL ANISOTROPY FROM LOCAL OBSERVATIONS
OF SHEAR-WAVE SPLITTING IN WEST BOHEMIA,
CZECH REPUBLIC

BY VÁCLAV VAVRYČUK

ABSTRACT

The results of a systematic study of shear-wave splitting, observed in the three-component digital seismograms of about 400 local microearthquakes that occurred during the 1985/1986 West-Bohemian earthquake swarm are presented. Two shear phases, polarized nearly perpendicularly in horizontal projection, were observed at all five stations of the local seismic network for most of the events. The polarization of the faster shear wave is aligned in the WNW – ESE direction, regardless of the mechanism and hypocenter location of the individual events, and coincides with the direction of the maximum horizontal compressive tectonic stress in the region. These effects are interpreted in terms of effective anisotropy of the upper crust in the region. The maximum delay time between the split shear waves is 0.15 sec and corresponds to 6% anisotropy.

Directional variation of the delay time was observed at the nearest station (epicentral distance ≈ 5 km). This variation was compared with functions predicted by theoretical models of cracked media to resolve which model is the most appropriate for crustal anisotropy. Surprisingly, no agreement could be found for Hudson's model of dry or water-filled parallel cracks that is widely used by many authors. A successful fit was obtained for Schoenberg — Douma's model of a medium with parallel fractures. The fracture normal pointed N31°E, and the optimum fracture parameters were $E_N = 0.4$ and $E_T = 0.02$. The theoretically calculated fractures are aligned parallel to the tectonic stress direction and do not correspond to any real tectonic lines in the region.

INTRODUCTION

A growing amount of seismic data indicates the existence of anisotropy in the upper crust. Of the various possible mechanisms of crustal anisotropy, the anisotropy associated with crustal tectonic stress and probably due to the presence of fracture systems with preferred orientation appears to be the most frequently observed (Crampin, 1978; 1981; 1984). Wave propagation in effectively anisotropic media has been studied both theoretically and experimentally. Theoretical calculations for media containing aligned circular cracks (Garbin and Knopoff, 1973; 1975a, b), ellipsoidal inclusions (Hudson, 1980; 1981; 1986; Nishizawa, 1982) and long, thin, parallel fractures (Schoenberg and Douma, 1988) predict transverse isotropy of the medium and infer its elastic properties from fracture parameters (e.g., crack density, aspect ratio, elastic parameters of material inside the cracks). Papers studying effective crustal anisotropy experimentally are based on the analysis of shear-wave splitting (Li *et al.*, 1988; Aster *et al.*, 1990; Kaneshima, 1990; Kaneshima *et al.*, 1990; Savage *et al.*, 1990; Shih and Meyer, 1990; Mjelde, 1991; Graham *et al.*, 1991; Sachpazi and Hirn, 1991). The orientation of the symmetry axis of transverse isotropy is deduced from polarization directions of split shear waves. The degree of anisotropy is estimated from the delay time between the split *S* waves, and ranges prevalingly from 3% to 10%.

It is desirable to determine the complete elasticity tensor that would allow the anisotropy predicted by different theoretical fracture models to be compared with that of the real structure. This comparison is crucial for a better understanding of the limits of applicability of simplified fracture models and for determining the fracture parameters of real structures. To determine the complete elasticity tensor, it is necessary to measure the delay time variations as a function of ray direction. The conditions that have to be satisfied to construct the directional delay time variation reliably are: (1) well-defined shear-wave splitting has to be observed to enable the interpreter to identify the S₂-wave unambiguously and to determine its arrival time correctly; (2) large number of data has to be available, because the delay times should be measured for a wide range of ray directions, and the rays should provide a dense coverage of the region being investigated.

These conditions are severe. This is evident, since no clear reliable directional variation of the delay time has been reported to date, although shear-wave splitting has been experimentally observed for almost ten yr.

Both conditions were satisfied in the case of the local observations of the 1985/1986 West-Bohemian earthquake swarm. These observations represent a data set exceptionally suitable for the above-mentioned purpose. In this paper the polarization directions of the split *S* waves are studied and the directional variation of the delay time is established. Finally, the fracture parameters are estimated and the complete elasticity tensor for the West Bohemia region is computed.

1985 / 1986 WEST-BOHEMIAN EARTHQUAKE SWARM

From December 1985 to January 1986, an earthquake swarm occurred in West Bohemia (see Fig. 1). Over 7000 weak, shallow earthquakes were recorded in its course; the local magnitudes of the two strongest being 4.6 and 4.1 (Neunhoefer *et al.*, 1989).

The hypocenters of the squarm occurred in the upper crust beneath the northeastern edge of the Cheb Basin, which is situated in the northwestern part of the Bohemian Massif (Fig. 2) and which developed during the Paleozoic and older orogenetic phases. The tectonic structure of the Tertiary Cheb basin represents the intersection of the Eger Graben, oriented WSW-ENE, and the Sudeten fault system running transversely to it (Dudek, 1987). The crystalline basement of the Cheb basin is covered by tertiary sediments with a maximum thickness of 400 m. Three main structural systems control the development of the basin (Šantrůček, 1986): the Sudeten NW-SE fault system, the Ore-Mountain WSW-ENE fault system, and the youngest N-S tectonic lines. The NW-SE fault system is best defined, being manifested by the Mariánské Lázně Fault, the azimuth of which is approximately 150°. The NW-SE and N-S structural trends, moreover, are also significant tectonic lines from the hydrogeological point of view, because they form the paths of ascent of mineral water and CO₂ from the basement of the basin. The present activity has been monitored by precise surveying that disclosed the lift of the eastern marginal block of the Cheb basin, and indicated that the Mariánské Lázně Fault is probably still active (Vyskočil and Kopecký, 1974).

The swarm activity was monitored by the local analog one-component stations Oloví (OLV), Klingenthal (KLI), Wernitzgruen (WRG) and Bad Elster (BDE), and local digital three-component stations Vackov (VAC), Tisová (TIS), Selb

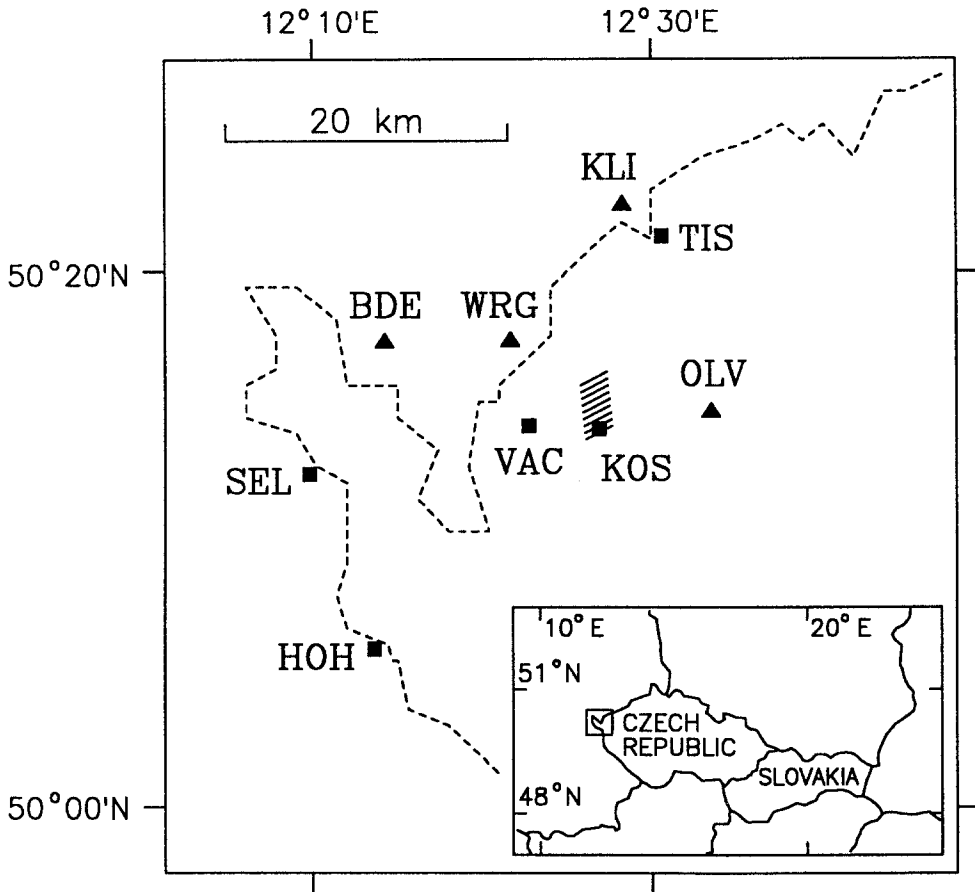


FIG. 1. Map of the West Bohemia region showing locations of digital (solid squares) and analog (solid triangles) seismic stations. The epicentral area is hatched.

(SEL), and Hohenberg (HOH) (Fig. 1). In addition, the permanent digital station Nový Kostel (KOS) was installed after the swarm to monitor the subsequent weak seismic activity of the region. The digital stations operated in the triggered mode. They were equipped with short-period SM-3 seismometers with a velocity-proportional output in a bandwidth of 0.6 to 30 Hz. The data were sampled at frequencies of 116 to 250 Hz and stored by Lennartz PCM-5800 recording equipment on PCM magnetic tapes. The effective dynamic range was above 100 dB (gain ranging used: 10-bit mantissa and 4-bit exponent). Detailed information about the stations can be found in Horálek and Jedlička (1987; VAC and KOS), Klimeš *et al.* (1987; TIS), and Neunhoefer *et al.* (1989; remaining stations).

Kolář and Vavryčuk (1990) located 143 events of the swarm by the FHYPO computer program (Herrmann, 1979). A simple model of a homogeneous, isotropic halfspace with $v_p = 5.76$ km/sec, constructed experimentally by Horálek *et al.* (1987), with different values of v_p/v_s was applied. Carefully reinterpreted P - and S -wave arrival times at stations VAC, TIS, and OLV (approximate epicentral distances of 5, 15, and 9 km, respectively) were used in the location procedure. The P (S) onset times were measured with an accuracy better than ± 0.01 sec (± 0.03 sec) for VAC and TIS and ± 0.05 sec (± 0.1 sec)

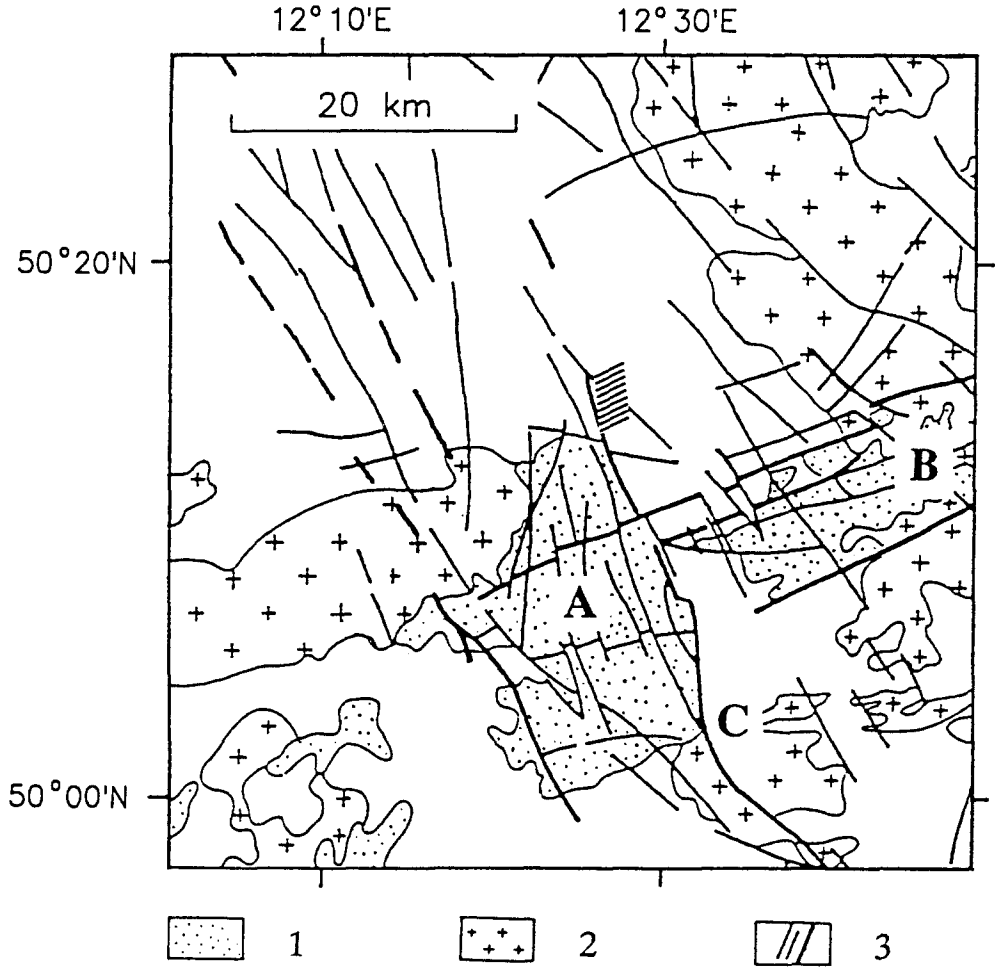


FIG. 2. Tectonic sketch of the West Bohemia region (after Dudek, 1987). (1) Tertiary basins; (2) Hercynian granitoid massifs; (3) faults; (A) Cheb Basin; (B) Ore-Mountain fault system; and (C) Mariánské Lázně fault. The epicentral area is hatched.

for OLV. The results show that the swarm activity was concentrated in a small elongated area. The earthquake epicenters form a belt, about 4 km long and 1 km wide, oriented nearly in the north-south direction (see Fig. 3). In the deep section, the hypocenters form a cluster, 1.5 km high dipping southward. The position of the focal area depends on the velocity model used. For low values of v_p/v_s the hypocenters shift to the south and to greater depths, for high values to the north and upward. The position does not change in the east-west direction. For $v_p/v_s = 1.62$ the hypocenters are located at depths of 8.5 to 10.5 km, for $v_p/v_s = 1.73$ at depths of 6 to 8 km. The north-south difference in positions between the two models amounts to about 1.5 km. The same dependence applies to changes in P -wave velocities at a constant v_p/v_s ratio.

POLARIZATION OF SPLIT S WAVES

Data and Method

The S -wave polarization was studied for selected events of the swarm recorded at stations VAC, TIS, SEL, and HOH and for selected events of the 1986 to 1990

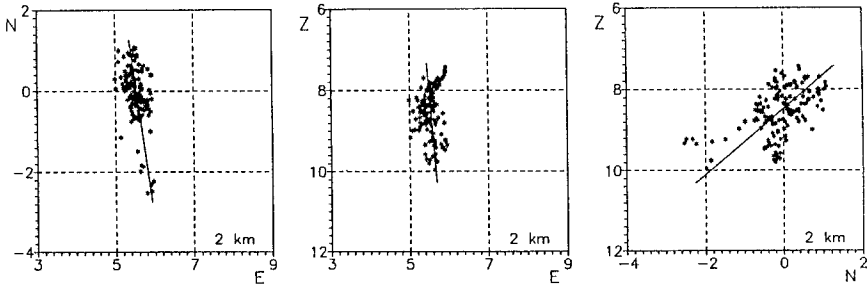


FIG. 3. Hypocenter projections of located events. The origin of Cartesian coordinates is placed at the VAC station. The velocity model with $v_p = 5.76$ km/sec and $v_p/v_s = 1.65$ was used. The solid line displays the prevailing direction of the belt of the hypocenters.

period, recorded at KOS. Events located by Kolář and Vavryčuk (1990) were used for VAC (141 events), TIS (139 events), and HOH (29 events). Stations SEL and KOS triggered poorly, therefore, all the recorded events, for which the signal-to-noise ratio was high enough to study *S*-wave polarization reliably, were used (23 events for SEL and 39 events for KOS).

All records were preprocessed by frequency filtering. The importance of frequency filtering is demonstrated in Figures 4a b. Figure 4a shows a three-component velocity seismogram of the event of 31 December 1985 at 04:39:34 (VAC, $M_L = 1.7$) with *P* and *S* waves plotted at an expanded timescale together with the respective polarization diagrams in horizontal projection. It is evident at first sight that the polarization diagrams are complicated and hardly interpretable. Figure 4b shows the numerically integrated record of the same event. The *P* waveform is dominated by a one-sided pulse, and the *S*-wave polarization displays a clear case of *S*-wave splitting. Because particle motion plots are simpler in displacement, the *S*-wave polarization was studied in ground displacement records.

The *S*-wave particle motions were plotted in horizontal projection and the prevailing polarization directions of the *S*1 and *S*2 waves were estimated by visual inspection. The analyst measured both polarization directions and assigned them to one of four classes according to their reliability. The first class consists of high-quality readings with an error of $\pm 5^\circ$. For the second class the error is about $\pm 10^\circ$. In the third class cases the polarization direction could be identified only approximately and the error is about $\pm 20^\circ$. The fourth class consists of events for which no prevailing polarization direction could be identified.

Results

The results of the analysis are presented in Figures 5 and 6, evaluated in Tables 1 and 2, and summarized in the following items.

- (1) All five stations recorded events with well-defined *S*-wave splitting. However, not all events displayed *S*-wave splitting. The *S*-wave polarization varied considerably for various events and from station to station in the same way as the delay times between two arriving *S* waves. In many cases the delay time was not long enough to separate the two *S* phases so that the polarization was the result of their interference. The polarization direction of the two *S* waves could thus only be estimated very roughly.

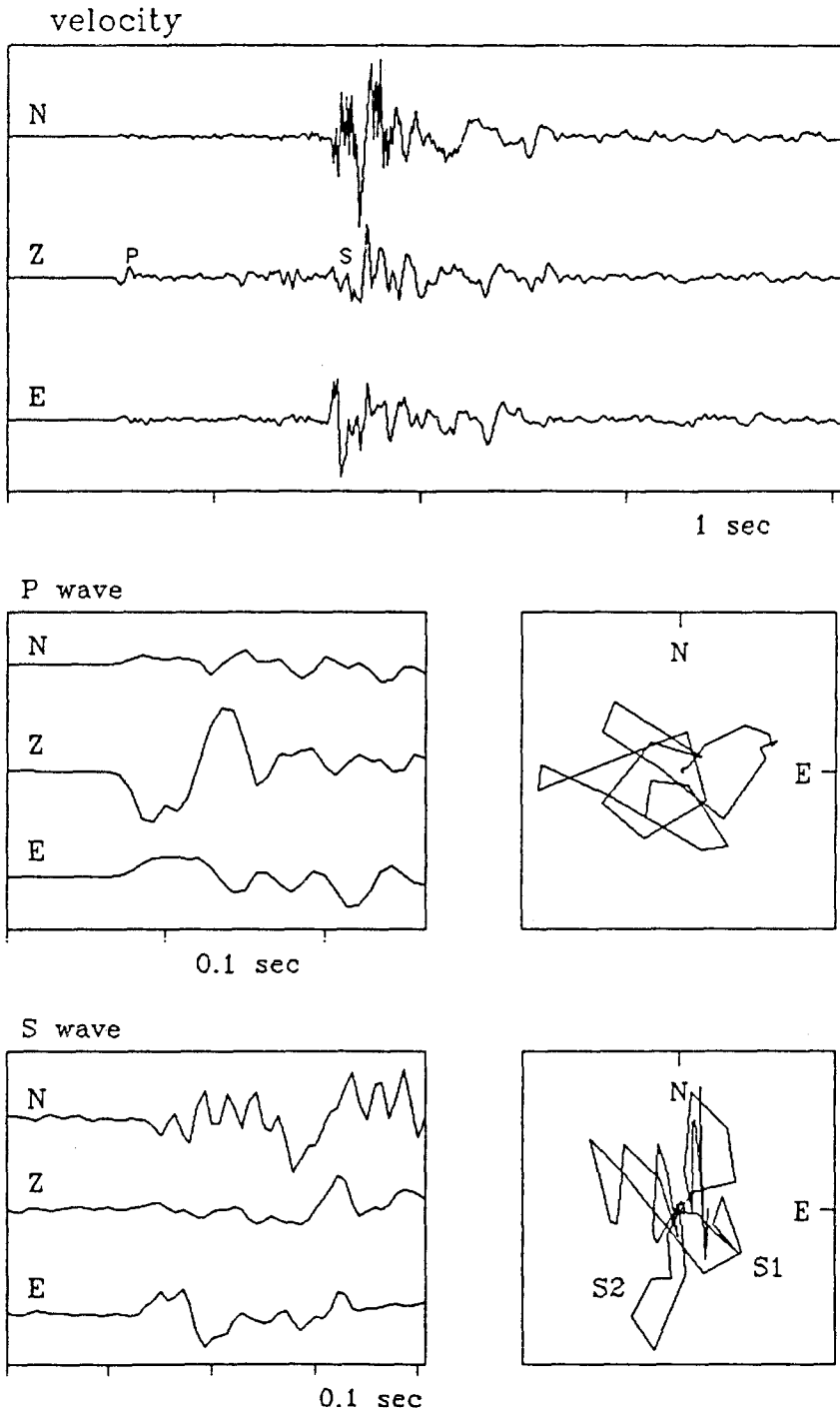


FIG. 4A. Three-component velocity seismogram of the event of 31 December 1985 at 04:39:34 (VAC, $M_L = 1.7$) with detailed *P* and *S* waveforms and polarization diagrams in horizontal projection.

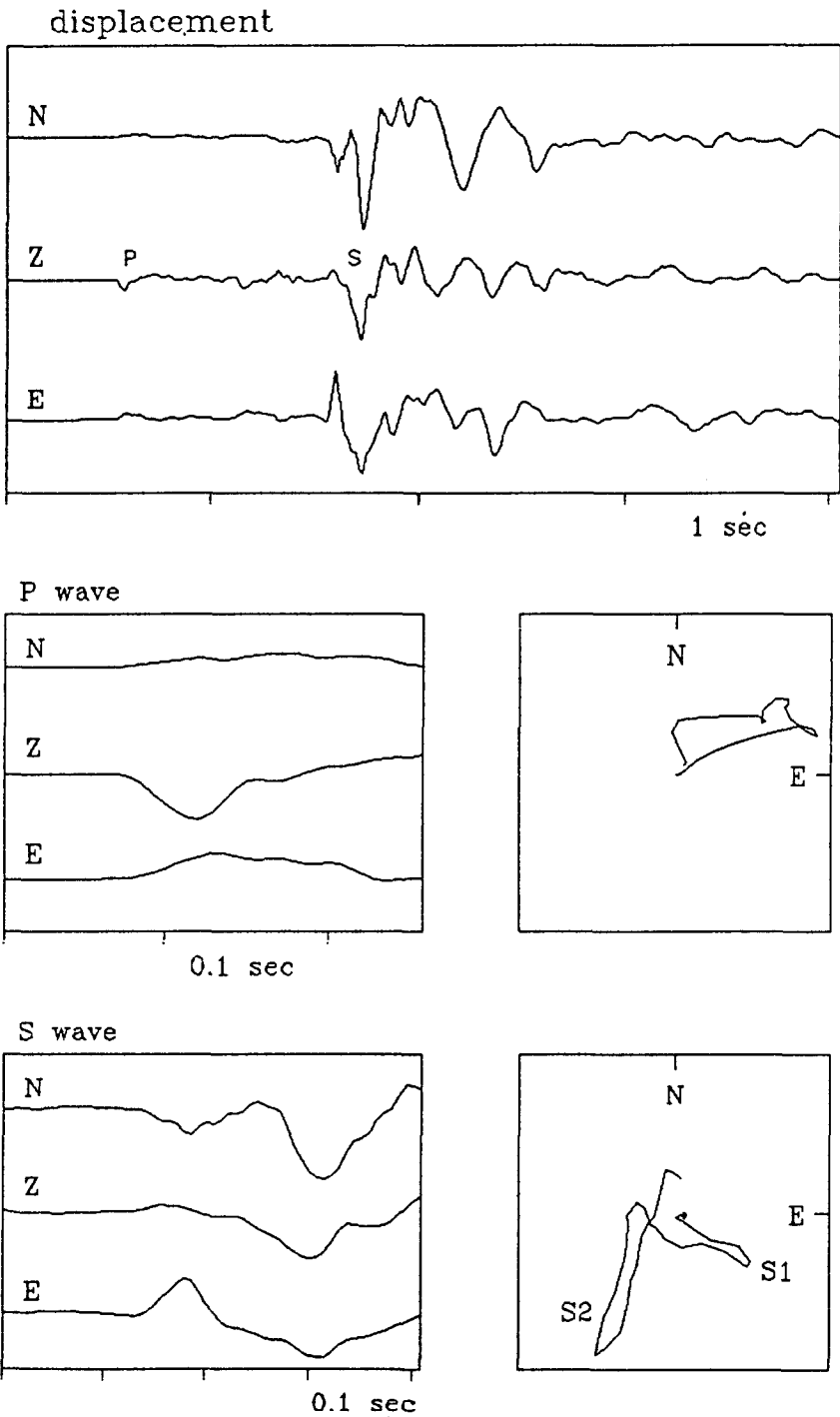
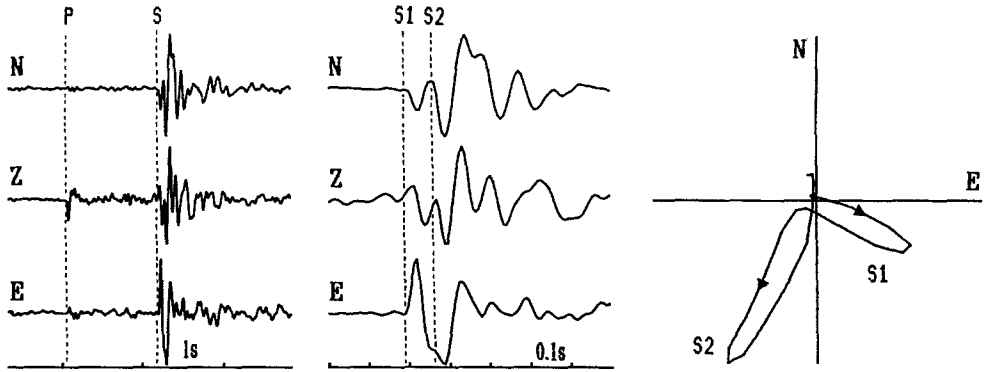
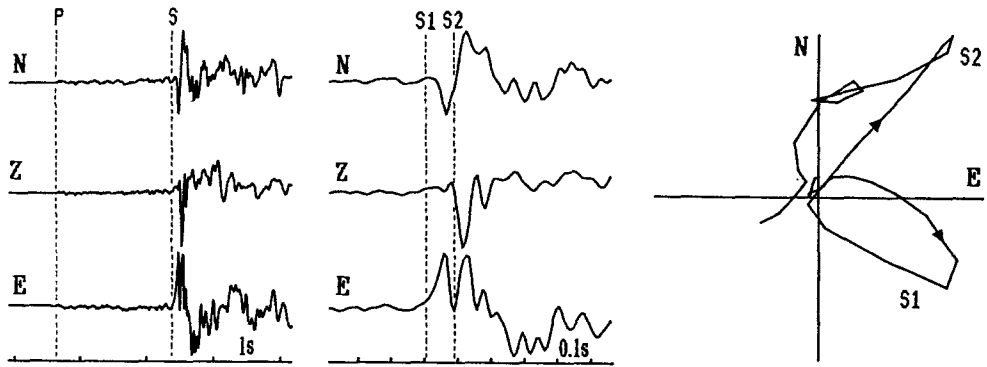


FIG. 4B. Three-component displacement seismogram of the event from Figure 4a obtained by numerical integration of the velocity records.

station: VAC



station: TIS



station: SEL

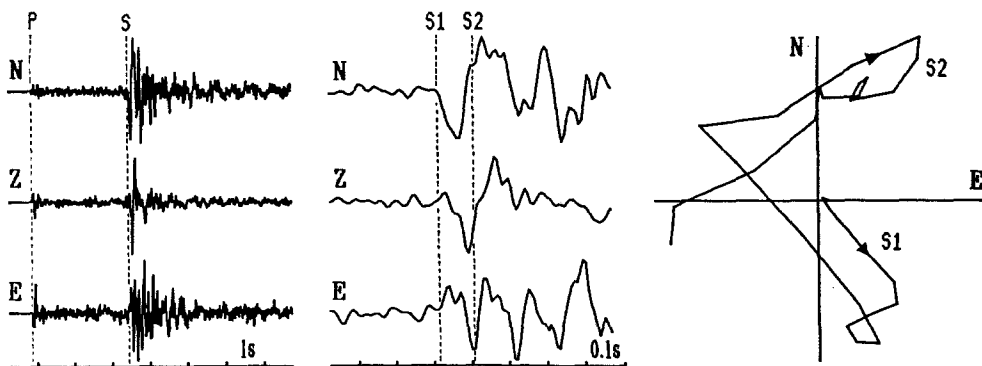
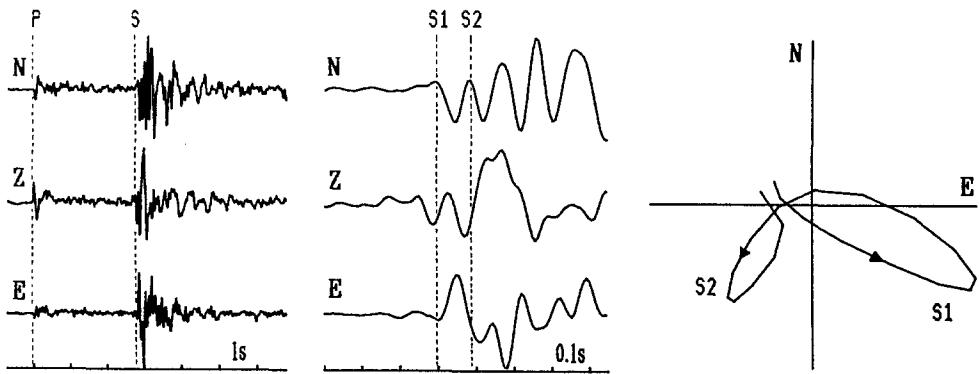
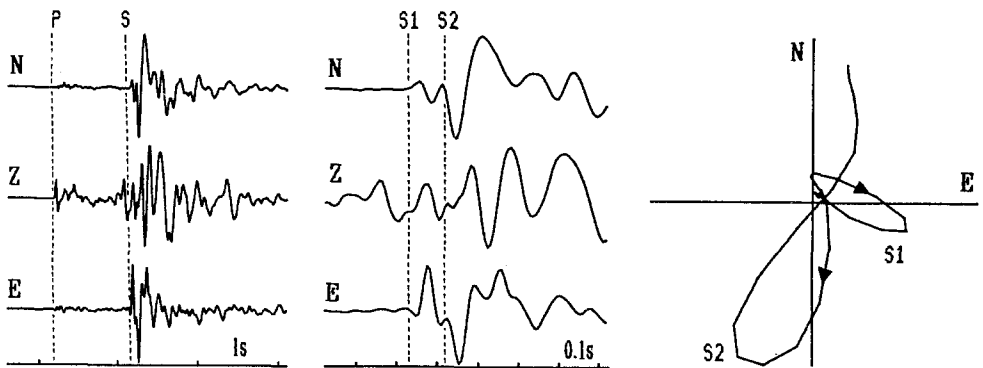


FIG. 5. Examples of distinct shear-wave splitting for five different events recorded by five different stations. A three-component seismogram is shown with marked P - and S -wave arrivals (*left*), the detail of an S -wave group with split S waves (*middle*) and the particle motions of the split S waves in the horizontal projection (*right*). Displacement records are presented for stations VAC, TIS, HOH, and KOS, and velocity record is shown for station SEL. For SEL the displayed event has a relatively long-period S wave; the split S waves are, therefore, separated better in the velocity record. The events of 30 December 1985 at 21:49:56 (SEL, $M_L = 2.5$), 20 January 1986 at 23:43:21 (VAC, $M_L = 1.2$), 23 January 1986 at 07:09:16 (HOH, $M_L = 1.6$), 6 February 1986 at 09:17:15 (TIS, $M_L = 2.6$) and 23 December 1989 at 21:23:50 (KOS, $M_L = 2.0$) were used.

station: HOH



station: KOS

FIG. 5. *Continued.*

- (2) The quality of the reading of polarization directions was station-dependent. The S1- and S2-wave could be best read at VAC and SEL, respectively. The scatter of measurements for both waves was least at VAC. The high reading error of the S2-wave polarization direction in some records is probably due to the above-mentioned interference of split S waves, which results in the contamination of the S2-wave arrival by the S1-wave.
- (3) The prevailing S1- or S2-wave polarization directions that could be measured were about the same for different stations and various events, although the mechanisms of some events evidently differed (different P-wave polarities at some stations).
- (4) The pie diagrams in Fig. 6 indicate that the scatter of polarization directions for a particular station is caused by reading error rather than by actual variation of the polarization directions for different events.
- (5) The more scattered values of the polarization directions, measured at more distant stations (SEL and HOH), are probably due to complex wave interaction with the surface: the waves reach these stations probably outside the shear-wave window. The averaged values of the polarization directions

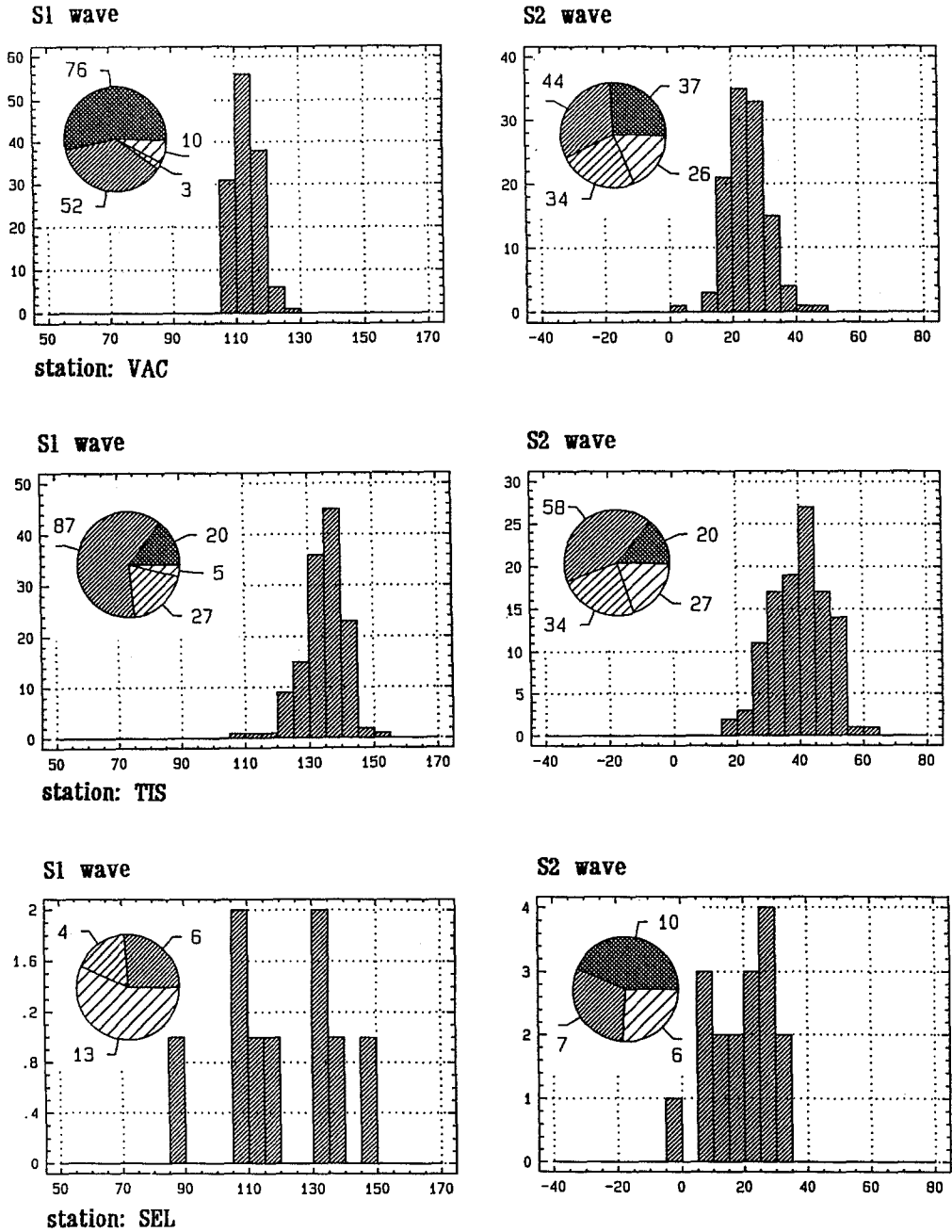


FIG. 6. Histograms of the polarization azimuths of the split waves and pie diagrams displaying the measurement quality of analysed events at a particular station. The azimuth was measured with an error of $\pm 5^\circ$ (1), $\pm 10^\circ$ (2), and $\pm 20^\circ$ (3), or no S-wave splitting was detected (4).

(Tables 1 and 2), however, coincide well with the values for the other stations. Therefore, these data were not removed from the analysis.

Anisotropy Hypothesis

The constant S1- and S2-wave polarization directions in horizontal projection, regardless of the station positions and event locations, indicate that the polar-

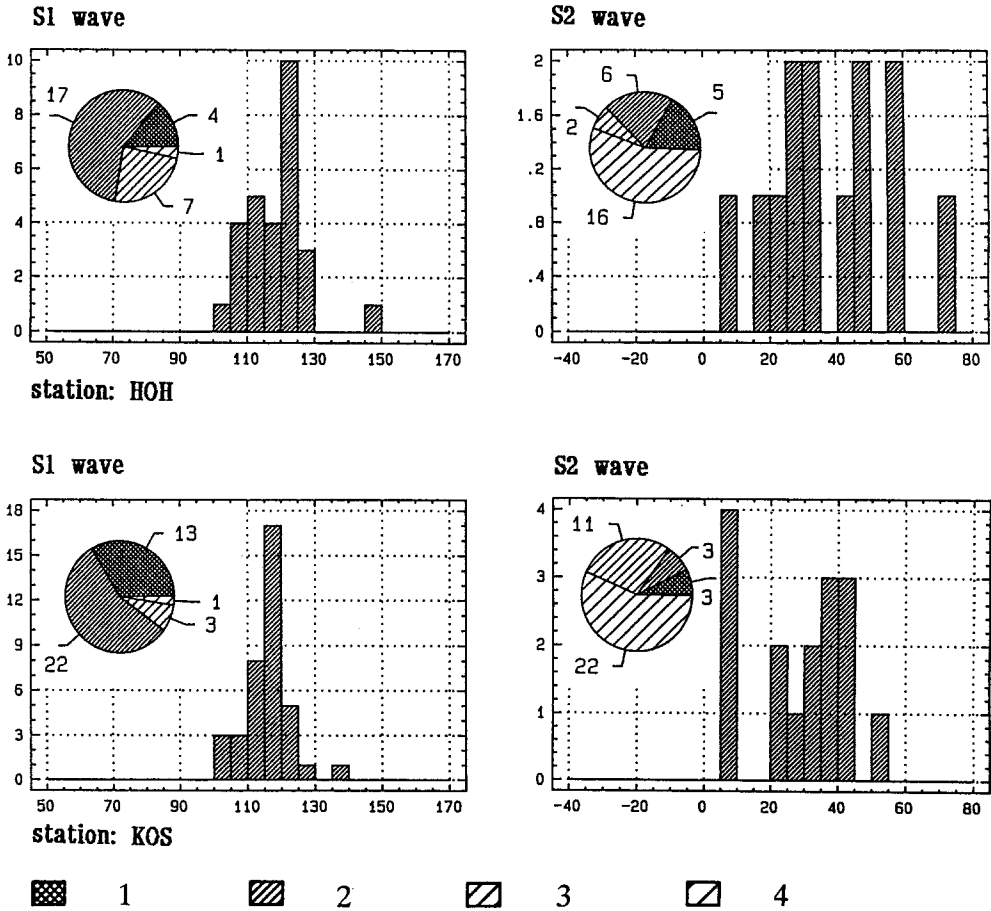


FIG. 6. Continued.

TABLE 1
S1-WAVE POLARIZATION DIRECTIONS

Station	N_1	N_2	a (°)	m (°)	δ (°)
VAC	141	132	114.1	114	3.9
TIS	139	134	135.3	136	6.6
SEL	23	9	121.0	117	17.9
HOH	29	28	119.3	120	9.1
KOS	39	38	116.7	118	6.9

$a_0 = 121^\circ$;

a = averaged value of the shear-wave polarization azimuth for a particular station; N_1 = number of analyzed events; N_2 = number of events for which the azimuth could be measured; m = median of the shear-wave polarization azimuth; δ = standard deviation; a_0 = averaged value of the shear-wave polarization azimuths for all stations.

TABLE 2
S2-WAVE POLARIZATION DIRECTIONS

Station	N_1	N_2	a (°)	m (°)	δ (°)
VAC	141	114	25.4	25	6.5
TIS	139	112	40.6	42	9.0
SEL	23	17	19.6	21	9.4
HOH	29	13	38.8	32	18.7
KOS	39	16	28.9	33	14.6

$\alpha_0 = 31^\circ$

For symbols see Table 1.

ization directions are not controlled by the focal mechanism. This observation can be consistently explained by the presence of a transversely isotropic medium with the axis of rotation symmetry in the horizontal plane (see Crampin, 1985). The S wave passing through this medium is split into two waves that propagate at different velocities and exhibit orthogonal polarizations. The direction of the horizontal symmetry axis can be inferred from the polarization of the split S waves and should coincide with the horizontal projection of the S1- or S2-wave polarization direction.

Upper crustal transverse isotropy with a horizontal axis of rotation symmetry is most frequently attributed to the presence of vertical parallel fracture systems in an isotropic medium. The fractures should be aligned parallel to the direction of the maximum horizontal compressive tectonic stress in the particular region, or close to it (Crampin *et al.*, 1984). Figure 7 shows a comparison of the stress direction in the West Bohemia region, determined by the hydraulic fracturing method (Rummel *et al.*, 1983), by the fault plane solution of the main swarm shock (Antonini, 1988) and by geodetic measurements of recent horizontal deformations (Vyskočil, 1987) with the S1-wave polarization direction. The polarization direction of the faster shear wave apparently correlates with the regional direction of stress. This result supports the hypothesis of stress-induced anisotropy in the region and indicates that the azimuth of the symmetry axis is probably $a = 31^\circ$.

DELAY TIME OF SPLIT S WAVES

Data and Method

The major problem in determining the delay time is to identify the S2-wave arrival reliably. The S2 wave is frequently superimposed on S1 or mixed with a number of secondary waves. The result is complex polarization in which the S2-wave onset is difficult to identify and the time delay difficult to measure. Currently, various methods are used for delay time determination (for an overview see MacBeth and Crampin, 1991): visual inspection, automated algorithms using the cross-correlation function of horizontal rotated components (Shih *et al.*, 1991), or variance tensor analysis (Aster *et al.*, 1990). The simplest method was used in this study. Using polarization diagrams the S2-wave arrival was picked up by an analyst at the time at which an abrupt change in the prevailing S1-wave polarization direction appeared. The author believes that it is not the method, but a large number of high-quality data that is decisive in successful determination of the delay time.

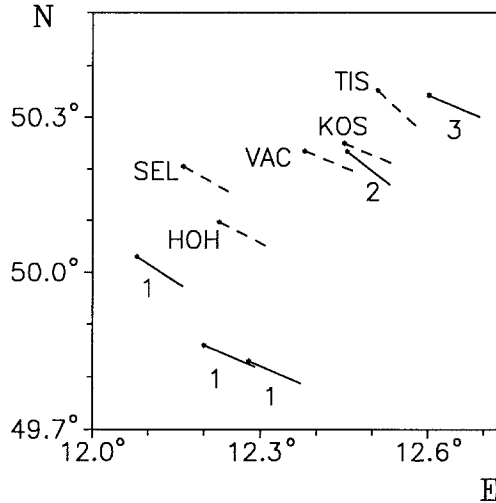


FIG. 7. Comparison of the maximum horizontal tectonic compressive stress direction in the epicentral region (solid line; 1: Rummel *et al.*, 1983; 2: Antonini, 1988; 3: Vyskočil, 1987) with the horizontal projection of the averaged S_1 -wave polarization directions (dashed line).

The records from VAC (epicentral distance about 5 km) are exceptionally suitable for shear-wave splitting analysis: the waveforms are very simple and display distinct shear-wave splitting. The seismometers were installed on a rock massif without sedimentary cover (Horálek and Jedlička, 1987), so that the seismograms are free of multiple reflections generated in subsurface layers. 249 swarm events were analyzed: in the first step the 141 events located by Kolář and Vavryčuk (1990), and in the second step another 108 events were added to provide dense coverage of the delay times for various ray directions. Incidence angles were determined for all the events from the apparent angles measured in the P -wave particle motions. The incidence angles are less than 25° , and thus all the events lie within the shear-wave window.

Ray Geometry

As mentioned above, the hypocenters of the swarm form a narrow belt, 4×1 km in area, directed north–south. The belt dips to the south. For simplicity, we will approximate the belt by a line that runs through its center. The line position and orientation depend on the parameters of the velocity model used in the location procedure. Because the model is not precisely defined, we considered four positions of the hypocenter line, obtained for four isotropic, homogeneous models with $v_p = 5.76$ km/sec and $v_p/v_s = 1.62$ (model 1), 1.65 (model 2), 1.69 (model 3), and 1.73 (model 4). The difference in the positions of the hypocenter line for models (1) and (4) amounts to 2.5 km in depth and 1.5 km (0.3 km) in the N–S (E–W) direction. Using the four alternative positions, we estimated the errors introduced into the ray direction calculations by inaccurate hypocenter locations.

The rays connecting the points distributed along the hypothetical line of hypocenters with the station form a set of straight lines (see Fig. 8) for which the directional variation of the delay time was studied. In a transversely isotropic medium it is sufficient to observe only its dependence on the ray

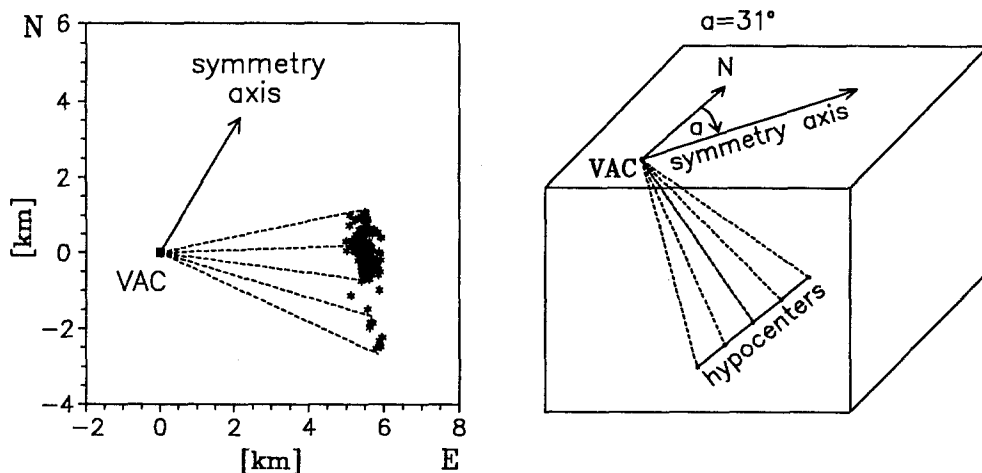


FIG. 8. Horizontal projection of rays connecting station VAC with epicenters (*left*; located for velocity model 2) and a spatial scheme of rays connecting VAC with the hypothetical line of hypocenters (*right*).

deviation from the symmetry axis (hereafter angle α). Figure 9 depicts α as a function of hypocenter position, which is uniquely determined by the difference in the arrival times of the P and S_1 waves (hereafter time t_{S-P}) at the station. The rays arriving at VAC cover approximately only one third of the entire angle interval 0° to 90° .

Results

The delay times between the split S waves range from 0.02 sec to 0.15 sec. Under the assumption that the structure is uniformly anisotropic along the entire ray length, for the estimated hypocentral distance $r = 8.8$ km and averaged S -wave velocity $v_S = 3.5$ km/sec the S -wave anisotropy amounts to 6%. However, this value is only the lower limit, because the measurement of the delay time does not include all the propagation directions, and thus it cannot be guaranteed that the delay time of $t_{S_2-S_1} = 0.15$ sec is really the maximum.

We sought variations of the delay time as a function of time t_{S-P} . Figure 10 shows that this function was successfully established and is nonlinear. The least-squares method was applied to 249 events to construct an averaged function. An exponential function in the form $t_{S_2-S_1} = \exp(a + b \cdot t_{S-P})$ was used to reproduce the observed nonlinear decay in data, and values $a = 3.89$ and $b = -5.90$ have been found. The decrease in the delay time for growing t_{S-P} (and thus also for growing hypocentral distance) is caused by the prominent dependence of the delay time on ray direction. To the author's knowledge it is *the first reliably measured dependence of the delay time on hypocenter position*.

Figures 9 and 10 enable us to determine the directional delay time variation, i.e., the delay time variation as a function of α (see Fig. 11). A new notation for the split shear waves— SP and SR waves—corresponding to the polarization directions, is introduced in Figure 11. The SP wave is the shear wave polarized in the plane defined by the ray and the symmetry axis, and the SR wave is polarized perpendicularly to that plane. Figure 11 indicates that the results are

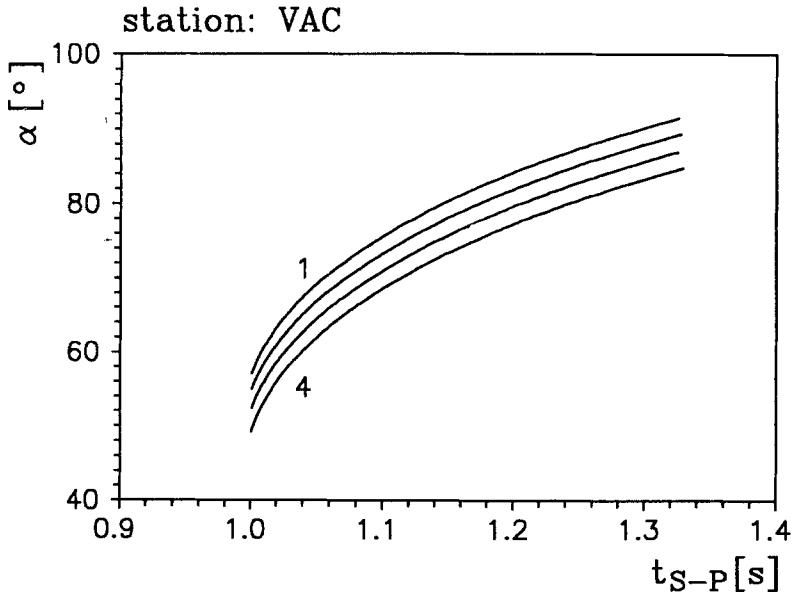


FIG. 9. Ray deviation from the symmetry axis as a function of t_{S-P} . The function is calculated for the hypocenters forming the hypothetical line for four alternative velocity models.

not very sensitive to the position of the hypocenter line. The alternative velocity models produce similar directional delay time functions that differ only slightly in slope and are only displaced a little in α . The errors introduced into the analysis by inaccurate hypocenter locations were suppressed by this lucky coincidence.

INVERSION FOR OPTIMUM FRACTURE MODEL

Inversion for transverse isotropy implies evaluating five independent elastic parameters in the coordinate system connected with the symmetry axis. Unfortunately, the inversion cannot be solved in general. The reason is the lack of observational data and nonlinearity of the problem. Therefore, we will simplify the problem and search for the optimum model only in transverse isotropies originating in fracture models. The advantage of these models consists of using estimated parameter values of the isotropic background as additional information for anisotropy inversion. In the following, we will search for the optimum model by comparing the observed directional delay time function with the theoretical functions generated by the most frequently used fracture models: Hudson's crack model (Hudson, 1980; 1981) and Schoenberg—Douma's fracture model (Schoenberg and Douma, 1988).

Hudson's Crack Model

Hudson's model of parallel cracks is described by the elastic parameters of an isotropic background, λ , μ , by crack density e , aspect ratio ϵ , and by the elastic parameters of the material contained in the cracks, λ' , μ' . We consider two types of cracks: dry cracks ($\lambda' = 0$, $\mu' = 0$) and water-filled cracks ($\lambda' = 2.25 \cdot 10^9 \text{ N/m}^2$, $\mu' = 0$) both nearly flat in shape ($\epsilon = 0.001$). The cracks are vertical and oriented parallel to the maximum horizontal tectonic stress, i.e., the azimuth of the crack normal is $\alpha = 31^\circ$. Value $e = 0.1$ is used for the crack

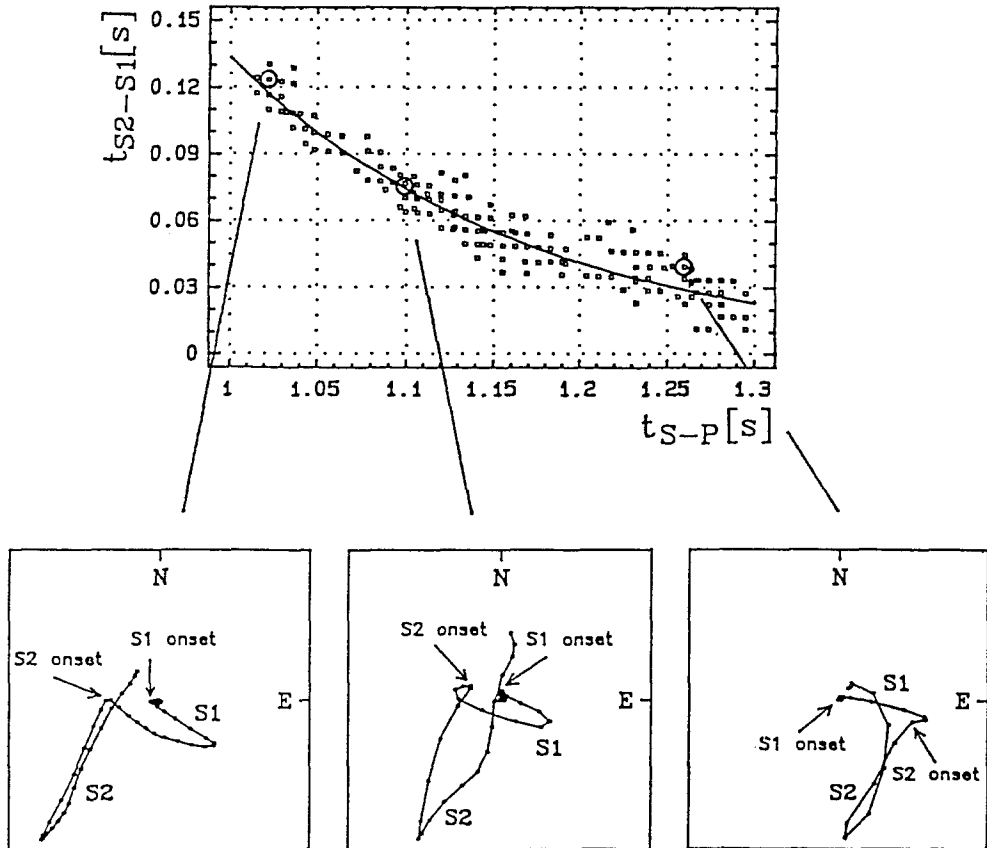


FIG. 10. t_{S2-S1} as a function of t_{S-P} for the VAC station with examples of shear-wave splitting for three events. The delay time was normalized to 1 sec of t_{S-P} . Particle motions in the horizontal projection show events (left): of 31 December 1985 at 1:23:44 ($M_L = 2.5$, $t_{S-P} = 1.02$ sec, $\Delta t = 7$ ms), 1 January 1986 at 4:45:29 ($M_L = 1.2$, $t_{S-P} = 1.10$ sec, $\Delta t = 7$ ms), 24 December 24, 1985 at 8:54:15 ($M_L = 1.0$, $t_{S-P} = 1.26$ sec, $\Delta t = 8$ ms). The distance between two points in particle motion represents the sampling interval Δt .

density, however, in the directional variation of the delay time this parameter only plays the role of a scaling factor and does not change its form. Values $\lambda = 31.3 \cdot 10^9$ N/m² and $\mu = 31.3 \cdot 10^9$ N/m² were applied for the isotropic background. These values were derived from the estimated velocity model in the West Bohemia region ($v_P = 5.76$ km/sec, $v_S = v_P/\sqrt{3}$, $\rho = 2.85 \cdot 10^3$ kg/m³).

Figure 12 shows that the theoretical delay time variation clearly disagrees with the observational data. In the angle interval of 50° to 90° the model predicts an increase in the delay time, but instead a drop is observed. For $\alpha = 90^\circ$ the theoretical delay time displays a maximum for both types of cracks. This property is preserved for all values of the crack parameters (see e.g., Douma, 1988; Peacock and Hudson, 1990), and thus the discrepancy between the observed and theoretical delay time function cannot be eliminated within the scope of Hudson's model of parallel cracks.

Schoenberg-Douma's Fracture Model

The model of a medium with parallel fractures is based on the idea of an isotropic medium containing a system of parallel internal fracture interfaces on

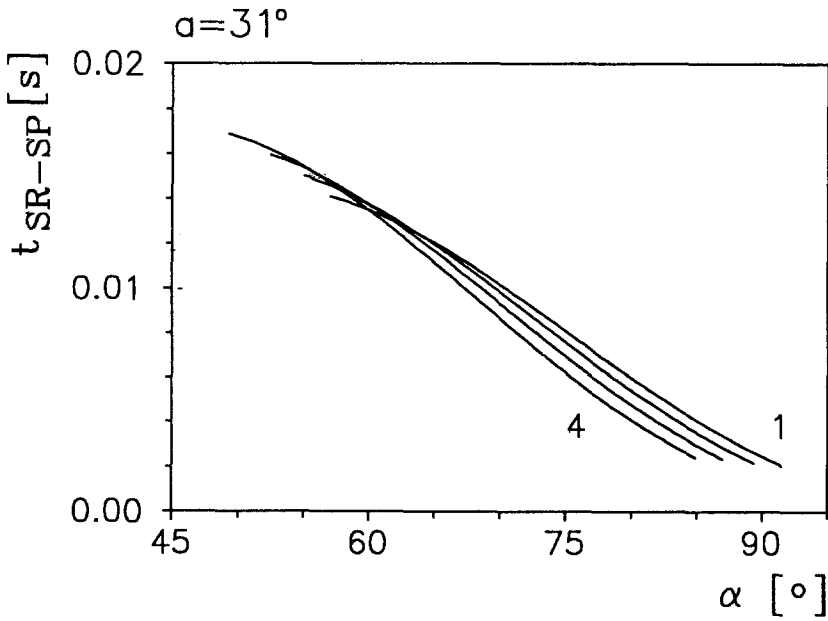


FIG. 11. Normalized delay time of the split *S* waves t_{SR-SP} as a function of the ray deviation from the symmetry axis.

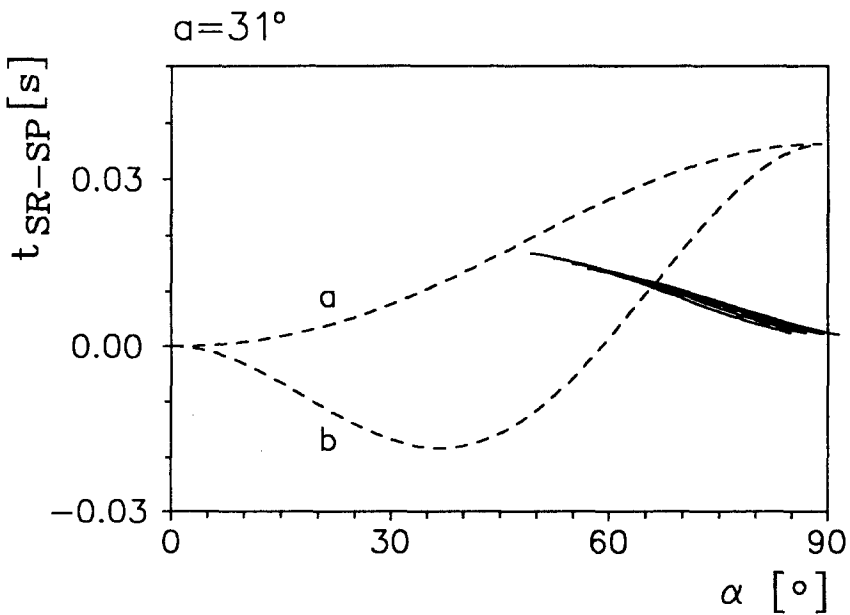


FIG. 12. Comparison of observed directional delay time variation (solid line) with theoretical functions (dashed line) calculated for Hudson's model of a medium with dry (a) and water-filled (b) parallel cracks. The delay time is normalized to 1 km of the ray length. Elements of Hooke's matrix (in $10^6 \text{ m}^2/\text{sec}$): dry cracks: $c_{11} = 31.4, c_{13} = 6.5, c_{33} = 19.4, c_{44} = 8.8, c_{66} = 11.0$; and water-filled cracks: $c_{11} = 32.9, c_{13} = 10.8, c_{33} = 32.4, c_{44} = 8.8, c_{66} = 11.0$.

which reversible displacements take place (Shoenberg and Douma, 1988). In this model, the computation of elastic coefficients of effective anisotropy involves the elastic coefficients of an isotropic background, λ , μ , and two fracture parameters, E_N , E_T . The fracture parameters are dimensionless constants characterizing the response of fractures to the normal and shear stress, respectively. The stability conditions on the fracture interfaces (see Douma, 1988) restrict E_N and E_T to nonnegative values only. For $E_N = 0$ and $E_T = 0$ the model degenerates to the isotropic medium without fractures.

Analogously to Hudson's model, we take $\lambda = 31.3 \cdot 10^9 \text{ N/m}^2$ and $\mu = 31.3 \cdot 10^9 \text{ N/m}^2$ as the isotropic background values, and the fractures are vertical with azimuth of the normal $\alpha = 31^\circ$. Figure 13a shows a comparison between the observational data and theoretical functions calculated for four fracture models: $E_N = 0.4$, $E_T = 0$ (model *a*), $E_N = 0.2$, $E_T = 0$ (model *b*), $E_N = 0$, $E_T = 0.2$ (model *c*), and $E_N = 0.2$, $E_T = 0.2$ (model *d*). Figure 13b gives a detailed comparison of the models with a good agreement with observations: $E_N = 0.3$, $E_T = 0$ (model 1), $E_N = 0.4$, $E_T = 0$ (model 2), and $E_N = 0.4$, $E_T = 0.02$ (model 3). A model within the range of models 1, 2, and 3, whose parameters are close to values $E_N = 0.4$, $E_T = 0.02$, can be considered the model that fits the experimental data best.

Hooke's matrix of this effectively anisotropic medium normalized by the medium density has the following form

$$C_{ij} = \begin{bmatrix} 23.5 & 7.8 & 7.8 & 0 & 0 & 0 \\ & 31.9 & 9.9 & 0 & 0 & 0 \\ & & 31.9 & 0 & 0 & 0 \\ & & & 11.0 & 0 & 0 \\ & & & & 10.8 & 0 \\ & & & & & 10.8 \end{bmatrix} \cdot 10^6 \text{ m}^2/\text{sec}^2.$$

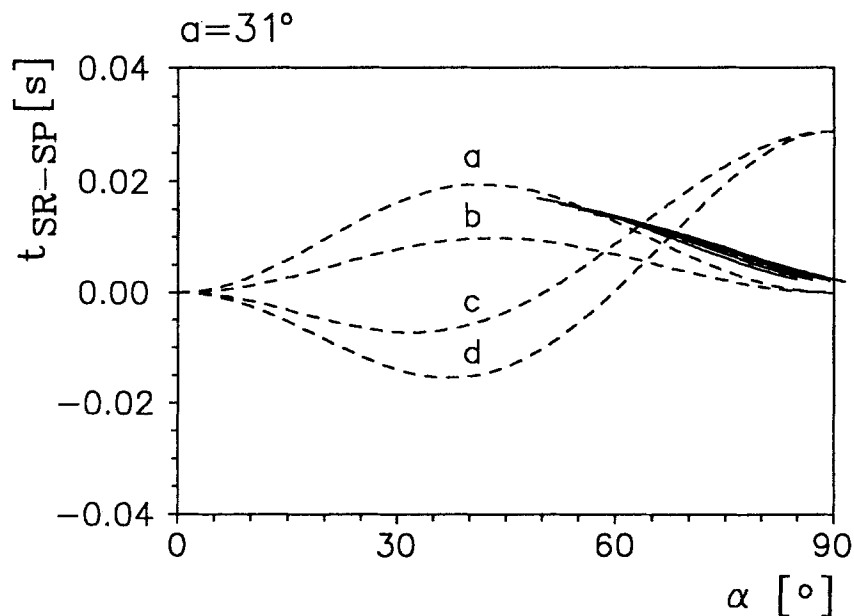
Matrix C_{ij} is specified in a coordinate system in which axis x coincides with the axis of rotation symmetry.

The following facts lend support to this optimum model. The behavior of the fracture interfaces as well as the resultant transverse isotropy are stable. The orientation of the symmetry axis corresponds to the idea of the presence of cracks or fractures parallel to the direction of the maximum horizontal tectonic stress in the West Bohemia region. The directional delay time function predicted by this model is in satisfactory agreement with the observed delay time function. The directional dependence of P - and S -wave velocities seems to be realistic (see Fig. 14)

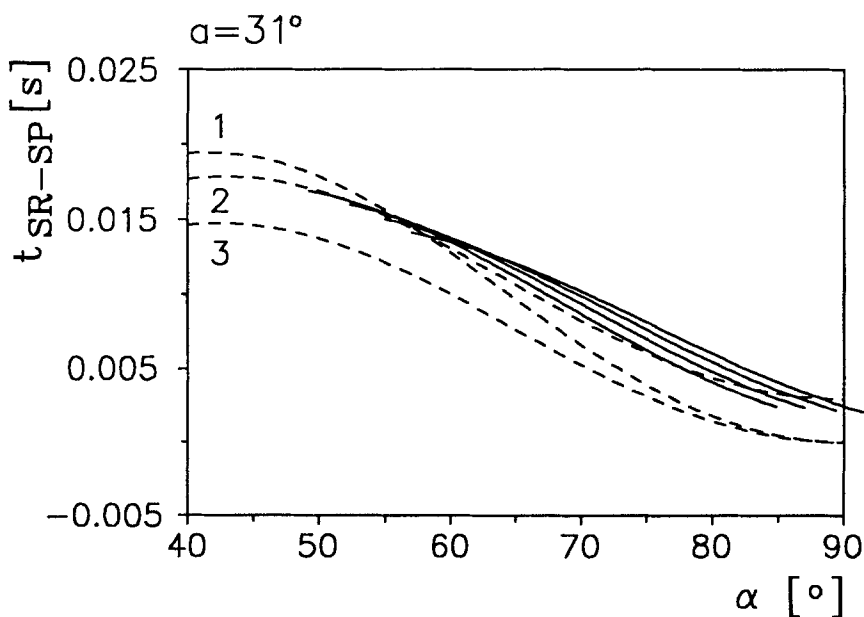
Geological Implications

We are now faced with the questions: How does the theoretical optimum fracture model correspond to the real structure? What can be deduced from this analysis about the existence and nature of real cracks or fractures in the geological structure of the West Bohemia region?

The theoretical model predicts parallel fractures oriented in the maximum tectonic stress direction. However, the theoretically calculated fractures deviate from the direction of the major fault system (see Fig. 2) by 30° , and thus the fractures cannot be simply identified with the faults in the region. Therefore, if the detected anisotropy is really induced by the cracks or fractures, the fractures should be of a much smaller size than the faults.



(a)



(b)

FIG. 13. Comparison of observed directional delay time variation (solid line) with theoretical functions calculated for the Schoenberg—Douma's fracture models. The delay time is normalized to 1 km of the ray length. Elements of Hooke's matrix (in $10^6 \text{ m}^2/\text{sec}^2$): model a: $c_{11} = 23.5$, $c_{13} = 7.8$, $c_{33} = 31.9$, $c_{44} = 11.0$, $c_{66} = 11.0$; model b: $c_{11} = 27.5$, $c_{13} = 9.2$, $c_{33} = 32.3$, $c_{44} = 11.0$, $c_{66} = 11.0$; model c: $c_{11} = 32.9$, $c_{13} = 11.0$, $c_{33} = 32.9$, $c_{44} = 11.0$, $c_{66} = 9.2$; and model d: $c_{11} = 27.5$, $c_{13} = 9.2$, $c_{33} = 32.3$, $c_{44} = 11.0$, $c_{66} = 9.2$. (b) Detailed comparison of observed directional delay time variation (solid line) with theoretical functions (dashed line) produced by models for which a qualitative fit was found. Elements of Hooke's matrix (in $10^6 \text{ m}^2/\text{sec}^2$): model 1: $c_{11} = 25.3$, $c_{13} = 8.4$, $c_{33} = 32.1$, $c_{44} = 11.0$, $c_{66} = 11.0$; model 2: $c_{11} = 23.5$, $c_{13} = 7.8$, $c_{33} = 31.9$, $c_{44} = 11.0$, $c_{66} = 11.0$; and model 3: $c_{11} = 23.5$, $c_{13} = 7.8$, $c_{33} = 31.9$, $c_{44} = 11.0$, $c_{66} = 10.8$.

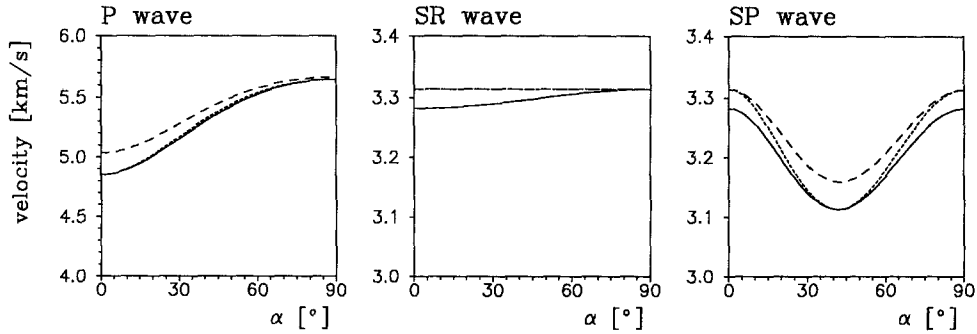


FIG. 14. Phase velocity of *P*, *SP*, and *SR* waves as a function of the direction of propagation for model 1 (dashed line), model 2 (dotted line), and model 3 (solid line) from Figure 13b.

Other information about the nature of the fractures, provided by the theoretical fracture model, concerns the type of contact between the fracture surfaces. The optimum fracture parameter values $E_N = 0.4$ and $E_T = 0.02$ indicate that the fractures are sensitive to normal stress, but display almost no response to shear stress. One of the possible explanations for this could be the irregularly roughened fracture interfaces, the sides of which are clenched each into the other.

CONCLUSION

The only satisfactory explanation of the *S*-wave splitting, observed in records of local events which occurred during the 1985/1986 West-Bohemian earthquake swarm, is effective transverse isotropy of the upper crust in the region. Transverse isotropy has a horizontal axis of rotation symmetry and causes approximately 6% anisotropy of *S* waves. The polarization direction of the fast shear wave, and thus also the direction of the symmetry axis, are apparently related to the direction of the maximum horizontal tectonic compressive stress in that region. Stress-induced anisotropy is accounted for by the presence of vertical parallel cracks or fractures, oriented in the direction of the acting tectonic stress. The reliably measured directional delay time variation enabled the author to perform the first ever test of applicability of theoretical fracture models to real structures.

It is proved that the commonly used Hudson model of dry or water-filled parallel cracks cannot be applied to the West Bohemia region, because it is unable to give a satisfactory explanation of the directional delay time variation. The failure of Hudson's crack model need not imply the absence of cracks in the geological structure, but more likely that the real crack behavior is not adequately described by this model. It could indicate that Hudson's model of parallel cracks inadmissibly simplifies the real crack geometry.

An optimum theoretical model fitting all the existing data was found with the aid of Schoenberg-Douma's fracture model. The model assumes an isotropic medium with velocities $v_p = 5.76$ km/sec and $v_s = v_p/\sqrt{3}$, that contains parallel vertical fractures with azimuth of the normal $\alpha = 31^\circ$. The values of the fracture parameters should be close to $E_N = 0.4$ and $E_T = 0.02$. This model has to be viewed as an approximate solution, which is only one of a variety of other possible solutions. The model, however, has the unique property that it is not

formal, it is in accordance with existing knowledge of the tectonic stress in the region, and it implicates realistic values of P - and S -wave velocities.

The geological interpretation of the proposed optimum model is not straightforward. The theoretically calculated fractures cannot be simply identified with surface tectonic lines in the West Bohemia region. It can be only hypothesized that the fractures, if they exist in the real geological structure and cause anisotropy, should be of a smaller size than the faults and should be prevalently oriented in the maximum horizontal tectonic stress. The fracture parameter values indicate, furthermore, that the fractures are not sensitive to shear stress but only to normal stress. This fact could be explained by fractures with irregularly roughened surfaces.

ACKNOWLEDGMENTS

The author thanks Vladislav Babuška, Axel Plešinger, and Ivan Pšenčík for their review and helpful comments, and M. Antonini and E. Schmedes for making available the data from the SEL and HOH stations.

REFERENCES

- Antonini, M. (1988). Variations in the focal mechanisms during the 1985/86 Western Bohemia earthquake sequence—correlation with spatial distribution of foci and suggested .
metry of faulting. In: *Induced Seismicity and Associated Phenomena*, Geophys. Inst., Czechosl. Acad. Sci., Praha, 250–270.
- Aster, R. C., P. M. Shearer, and J. Berger (1990). Quantitative measurements of shear wave polarizations at the Anza seismic network. Southern California: implications for shear wave splitting and earthquake prediction. *J. Geophys. Res.* **95**, 12,449–12,473.
- Crampin, S. (1978). Seismic wave propagation through a cracked solid: polarization as a possible dilatancy diagnostic, *Geophys. J. R. Astr. Soc.* **53**, 467–496.
- Crampin, S. (1981). A review of wave motion in anisotropic and cracked elastic media, *Wave Motion* **3**, 343–391.
- Crampin, S. (1984). Effective anisotropic elastic constants for wave propagation through cracked solids, *Geophys. J. R. Astr. Soc.* **76**, 135–145.
- Crampin, S., R. Evans, and B. K. Atkinson (1984). Earthquake prediction: a new physical basis, *Geophys. J. R. Astr. Soc.* **76**, 147–156.
- Crampin, S. (1985). Evaluation of anisotropy by shear-wave splitting, *Geophysics* **50**, 142–125.
- Douma, J. (1988). The effect of the aspect ratio on crack-induced anisotropy, *Geophys. Prospect.* **36**, 614–632.
- Dudek, A. (1987). Geology and tectonic pattern of the western Bohemia seismic area. In: *Earthquake Swarm 1985/86 in Western Bohemia*, Geophys. Inst., Czechosl. Acad. Sci., Praha, 132–141.
- Garbin, H. D., and L. Knopoff (1973). The compressional modulus of material permeated by a random distribution of circular cracks, *Q. Appl. Math.* **30**, 453–464.
- Garbin, H. D. and L. Knopoff (1975a). The shear modulus of material permeated by a random distribution of free circular cracks, *Q. Appl. Math.* **33**, 296–300.
- Garbin, H. D. and L. Knopoff (1975b). Elastic moduli of a medium with liquid-filled cracks, *Q. Appl. Math.* **33**, 301–303.
- Graham, G., S. Crampin, and L. M. Fernandez (1991). Observations of shear-wave polarizations from rockbursts in a South African gold field: and analysis of acceleration and velocity recordings, *Geophys. J. Int.* **107**, 661–672.
- Herrmann, R. B. (1979). Fasthyp—a hypocenter location program, *Earthq. Notes* **50**, 25–38.
- Horálek, J. and P. Jedlička (1987). Temporary three component digital seismic stations Vackov and Nový Kostel. In: *Earthquake Swarm 1985/86 in Western Bohemia*, Geophys. Inst., Czechosl. Acad. Sci., Praha., 132–141.
- Horálek, J., V. Vavryčuk, A. Plešinger, I. Pšenčík, P. Jedlička, and J. Soukup (1987). Refined localization of selected Jan. 5–Feb. 6, 1986 events of the West-Bohemian earthquake swarm. In: *Earthquake Swarm 1985/86 in Western Bohemia*, Geophys. Inst., Czechosl. Acad. Sci., Praha, 226–235.

- Hudson, J. A. (1980). Overall properties of a cracked solid, *Math. Proc. Camb. Phil. Soc.* **88**, 371–384.
- Hudson, J. A. (1981). Wave speeds and attenuation of elastic waves in material containing cracks, *Geophys. J. R. Astr. Soc.* **64**, 133–150.
- Hudson, J. A. (1986). A higher order approximation to the wave propagation constants for a cracked solid, *Geophys. J. R. Astr. Soc.* **87**, 265–274.
- Kaneshima, S. (1990). Origin of crustal anisotropy: shear wave splitting studies in Japan, *J. Geophys. Res.* **95**, 11.121–11.133.
- Kaneshima, S., N. Maeda, and M. Ando (1990). Evidence for the splitting of shear waves from waveforms and focal mechanism analyses, *Phys. Earth Planet. Interiors* **61**, 238–252.
- Klimes, L., P. Mohapl, V. Rudajev, and B. Růžek (1987). Data on the earthquake swarm in Western Bohemia recorded by the seismographic station Tisová-Helena. In: *Earthquake Swarm 1985/86 in Western Bohemia*, Geophys. Inst., Czechosl. Acad. Sci., Praha, 314–327.
- Kolář, P. and V. Vavryčuk (1990). *Reinterpretation of Selected Events of West-Bohemian Earthquake Swarm 1985-86*, Report of Geophys. Inst., Czechosl. Acad. Sci., Praha.
- Li, Y.-G., P. C. Leary, and T. L. Henyey (1988). Stress orientation inferred from shear wave splitting in basement rock at Cajon Pass, *Geophys. Res. Lett.* **15**, 997–1000.
- MacBeth, C. and S. Crampin (1991). Comparison of signal processing techniques for estimating the effects of anisotropy, *Geophys. Prospect.* **39**, 357–385.
- Mjelde, R. (1991). Analysis of shear waves with respect to splitting near the San Andreas Fault, *Geophys. J. Int.* **107**, 649–660.
- Neunhoefer, H., D. Gueth, D. Procházková, V. Tobyáš, J. Soukup, R. Michek, D. Knaislová, V. Vavryčuk, J. Zedník, P. Jedlička, J. Horálek, F. Čermák, E. Schmedes, M. Antonini, V. Bucha, L. Klimes, P. Mohapl, B. Růžek, and W. Strauch (1989). *Earthquake Swarm 1985/86 in Western Bohemia: Joint Bulletin of Local Seismological Stations*, Geophys. Inst., Czechosl. Acad. Sci., Praha 1989.
- Nishizawa, O. (1982). Seismic velocity anisotropy in a medium containing oriented cracks—transversely isotropic case, *J. Phys. Earth* **30**, 331–347.
- Peacock, S. and J. A. Hudson (1990). Seismic properties of rocks with distributions of small cracks, *Geophys. J. Int.* **102**, 471–484.
- Rummel, F., J. Baumgaertner, and H. J. Alheid (1983). Stress measurements along the eastern boundary of the SW-German block. In: *Proceedings of Workshop on Fracturing Stress Measurements*, Natl. Academy Press, Washington, DC, 3–17.
- Sachpazi, M. and A. Hirn (1991). Shear-wave anisotropy across the geothermal field of Milos, Aegean volcanic arc, *Geophys. J. Int.* **107**, 673–686.
- Savage, M. K., W. A. Peppin, and U. R. Vetter (1990). Shear wave anisotropy and stress direction in and near Long Valley Caldera, California, 1979–1988, *J. Geophys. Res.* **95**, 11.165–11.177.
- Shih, X. R. and R. P. Meyer (1990). Observation of shear wave splitting from natural events: South Moat of Long Valley Caldera, California, June 29 to August 12, 1982, *J. Geophys. Res.* **95**, 11.179–11.195.
- Shih, X. R., J. F. Schneider, and R. P. Meyer (1991). Polarities of P and S waves, and shear wave splitting observed from the Bucaramanga Nest, Colombia, *J. Geophys. Res.* **96**, 12.069–12.082.
- Schoenberg, M., and J. Douma (1988). Elastic wave propagation in media with parallel fractures and aligned cracks, *Geophys. Prospect.* **36**, 571–590.
- Šantrůček, P. (1986). Hlavní strukturní rysy chebské terciérní oblasti (in Czech with English abstract). In: *Computer Processing of Data from Czechoslovak Seismic Network*, 22–30, Bratislava.
- Vyskočil, P. and A. Kopecký (1974). *Neotectonics and recent crustal movements in the Bohemian Massif*, Edice Výzk. úst. geodet., top. a kart., Praha, 179 pp.
- Vyskočil, P. (1987). Horizontal recent tectonic deformations in Western Bohemia. In: *Earthquake Swarm 1985/86 in Western Bohemia*, Geophys. Inst., Czechosl. Acad. Sci., Praha., 388–390.

GEOPHYSICAL INSTITUTE
CZECH ACADEMY OF SCIENCE
BOČNÍ II / 1401
14131 PRAGUE, CZECH REPUBLIC

Manuscript received 27 March 1992